ACS APPLIED MATERIALS & INTERFACES

Research Article

www.acsami.org

Investigation of $CuInS_2$ Thin Film Formation by a Low-Temperature Chemical Deposition Method

Achim Fischereder,[†,‡] Thomas Rath,*[,†,‡] Wernfried Haas,[‡,§] Heinz Amenitsch,[⊥] Dorith Schenk,[†] Armin Zankel,[§] Robert Saf,[†] Ferdinand Hofer,[§] and Gregor Trimmel*[,†,‡]

[†]Institute for Chemistry and Technology of Materials, Graz University of Technology, Stremayrgasse 9, 8010 Graz, Austria

[‡]Christian Doppler Laboratory for Nanocomposite Solar Cells, Graz University of Technology and NanoTecCenter Weiz Forschungsgesellschaft mbH, Austria

[§]Institute for Electron Microscopy and Fine Structure Research, Graz University of Technology, Steyrergasse 17, 8010 Graz, Austria

[⊥]Institute of Biophysics and Nanosystems Research, Austrian Academy of Sciences, Schmiedlstraße 6, 8010 Graz, Austria

Supporting Information

ABSTRACT: Copper indium disulfide ($CuInS_2$, CIS) thin films were prepared by an alternative solution-based coating process adapted from the well-established aqueous metal salt/thiourea precursor system. The temperature for the decomposition of the precursors and the formation of CIS was lowered significantly to 130 °C by using the strongly coordinating solvent pyridine instead of the commonly used water. In addition, the influence of different annealing temperatures and concentrations of thiourea (TU) in the precursor solution on the obtained CIS samples was investigated. The films possess highly beneficial properties for photovoltaic applications, showing a chalcopyrite crystal structure, a high optical absorption (>10^4 cm^{-1}) and an optical band gap between 1.45 and 1.51 eV. Chemical and morphological changes during the thin film formation were detected and explained by time-resolved simultaneous grazing incident small- and wide-angle X-ray scattering (GISAXS, GIWAXS) measurements, scanning electron microsccopy (SEM) and simultaneous thermogravimetry/mass spectroscopy (TG/MS).

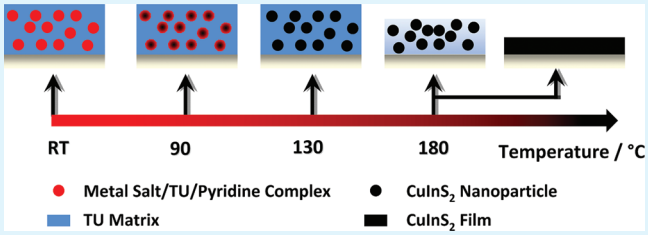

KEYWORDS: *copper indium disulfide, chemical deposition method, GISAXS, GIWAXS*

INTRODUCTION

Thin films of $CuInS_2$ (CIS) have attracted significant academic and industrial interest in the past few years because of their beneficial properties for various optoelectronic applications, especially in the field of photovoltaics.[1−3] CIS, a ternary semiconductor (I−III−IV_2), contains nontoxic constituents and exhibits a near optimum direct band gap of approximately 1.5 eV,[4] allowing a calculated theoretical photovoltaic conversion efficiency of 28.5%.[5] In addition, it is also possible to choose between n- and p-type conductivity by varying the elemental composition of the material.[1] In the literature numerous methods, e.g., thermal evaporation,[6,7] sulfurization of metallic precursors,[8] rf sputtering,[9,10] or chemical vapor deposition,[11,12] can be found to prepare such semiconducting thin films. However, many of them are not capable for scale up at low costs. From the economic point of view chemical deposition methods, especially spray pyrolysis processes, offer an attractive solution to this problem, as large area thin films can easily be prepared. The majority of these chemical deposition methods use thiourea (TU) as sulfur source and none-coordinating or only weak coordinating solvents like H_2O to dissolve the metal salt precursors.[13−18] Efficiencies of 9.5% were already achieved for an all sprayed $CuInS_2/In_2S_3$-solar cell,[18] however, temperatures of 300 °C have to be applied to form the ternary semiconductor.[16,17,19−22] A lowering of the temperature for the preparation of the solar absorber layer to about 150 − 200 °C would open the possibility to produce solar cell layers on cheap and flexible polymer substrates (e.g., PET, PEN), which would pave the way for a fast and cost-effective roll to roll solar cell fabrication similar to polymer-based solar cells.[23,24] Detailed studies of the thermal behavior of metal-thiourea complexes prepared from aqueous solutions revealed that the corresponding metal sulfides ($CuInS_2$, CuS, and ZnS) were only formed at temperatures above 200 °C,[25,26] which corresponds to the decomposition temperature of thiourea (approximately 190 °C).[27]

In the present work, we investigate an alternative solution-based coating process for the preparation of CIS layers adapted from the metal salt/thiourea precursor system, but in our case we use pyridine as solvent. Pyridine, as a coordinating solvent, offers the possibility to influence the decomposition of the precursors catalytically, which was shown for the preparation of CuS, starting from $CuCl_2$ and TU before.[28] A similar effect was observed for the decomposition of alkyl xanthates too, where

Received: October 21, 2011
Accepted: December 1, 2011
Published: December 1, 2011

alkylamine solvents caused a significant decrease in the decomposition temperature because of their coordinating ability.[29]

Within this work, the influence of different annealing temperatures and amounts of thiourea was evaluated with various analytical methods: X-ray diffraction (XRD), optical absorption spectroscopy, and energy-dispersive X-ray spectroscopy (EDX). In addition, the early stages of the CIS formation in the thin films were investigated in detail by an in situ time- and temperature-resolved synchrotron X-ray analysis. To obtain further information, a simultaneous thermogravimetric/mass spectroscopy (TG/MS) analysis was performed and additionally prepared CIS samples were analyzed with high-resolution mass spectroscopy (HRMS) to identify remaining impurities.

EXPERIMENTAL SECTION

Chemicals. Copper(I) acetate (CuAc, 97%), indium(III) chloride ($InCl_3$, 98%), thiourea (TU, 99%) and pyridine (reagent plus ≥99%) were purchased from Sigma Aldrich and used without further purification.

Indium tin oxide- (ITO)-coated glass substrates with a surface resistivity of 15−25 ohm/cm^2 were purchased from Delta Technologies Ltd.

Sample Preparation. ITO-coated glass substrates were cleaned in an ultrasonic water bath followed by an ultrasonic isopropanol bath, each for 20 min. The CIS precursor solution consisted of CuAc (0.22 mol/L), $InCl_3$ (0.15 mol/L), and TU (0.6 mol/L, 1.05 mol/L or 1.5 mol/L) dissolved in pyridine. On the basis of the assumptions that CIS with the formula Cu_xIn_yS $((x/2)+(2y/3))$ is formed and that each TU molecule provides one S atom, the TU concentrations correspond to 1.8, 3.1, and 4.5 equiv. of TU, respectively. The solution was spin coated on the substrates at a speed of 1000 rpm. The obtained films were annealed for 30 min at different temperatures in the range of 160−450 °C under vacuum. After the heat treatment, the samples were cooled to room temperature under vacuum within 10 min.

For XRD analysis, TEM-EDX measurements and HRMS studies the CIS-precursor solution was sprayed onto glass substrates at ambient conditions, followed by the same heat treatment of the substrates as described above. Finally, the thick CIS layer was scraped off the glass substrate to obtain a CIS powder.

For TG/MS measurements 25 μL of the CIS-precursor solution was transferred into an Al_2O_3 crucible, which was further stored under vacuum at 60 °C for 8 h prior the measurement.

Characterization. The X-ray powder diffraction profiles were measured with a Siemens D-5005 powder diffractometer (θ/θ geometry, Cu K_α radiation, graphite monochromator, scintillation counter, step width 0.02°, constant counting times of 10 s/step, measured range of 10−70° in 2θ). Transmittance and reflectance spectra of the thin films were measured with a Lambda 900 spectrometer (Perkin-Elmer) including an external integrating sphere diffuse reflectance accessory (PELA-1000). The film thickness was measured with a Veeco Dektak 150 surface profiler. Scanning electron microscopy images were recorded at 15 kV with a Zeiss Ultra 55 using a SE-inlens (SE) detector and an angle selective backscattered electron (ASB)-detector. Energy dispersive X-ray (EDX) spectra were recorded in scanning transmission electron microscopy (STEM) mode using a Philips CM20/STEM (200 kV, LaB_6 cathode, Noran HPGe-detector). Simultaneous 2D grazing incident small-angle X-ray scattering (GISAXS) and 1D gracing incident wide-angle X-ray scattering (GIWAXS) measurements were performed at the Austrian SAXS Beamline 5.2 L of the electron storage ring ELETTRA (Italy).[30] The beamline has been adjusted to a q-resolution ($q = 4\pi/\lambda\sin(2\theta/2)$) between 0.1 and 3.1 nm^{-1} (GISAXS) and to resolve the angular range (2θ) between 21.1 and 41.8° (GIWAXS) a X-ray energy of 8 keV was used. The samples were placed in a custom-made sample cell with a grazing angle of about 0.18° and were heated from 40 °C up to 190 °C at a heating rate of approximately 8 °C min^{-1} under vacuum. During the temperature scan, data were recorded with 5 and 10 s resolution for GISAXS using an image intensified CCD detector (model CV 12, Photonic Science Ltd., Millham/UK) and GIWAXS using a 1-D gas detector based on the delay line principle, respectively.[31] The simultaneous TG/MS measurements were carried out with a Netzsch STA 449C thermal analyzer under helium atmosphere and the helium flow was fixed at 50.0 mL min^{-1}. The samples were held at 20 °C for 10 min, then heated up with a rate of 8 °C min^{-1} followed by an isothermal step at 550 °C for 10 min. The volatile products of the thermal decomposition were analyzed online with a Netzsch QMS 403C quadrupole mass spectrometer. High resolution mass spectrometry (HRMS) studies of CIS powders were carried out with direct insertion mass spectrometry (DI-MS) with electron impact (EI, 70 eV) on a Waters GCT Premier.

RESULTS AND DISCUSSION

Sample Preparation. Precursor solutions were prepared from metal salts (copper(I) acetate, indium(III) chloride) and thiourea (TU) in pyridine. To investigate the influence of the annealing temperature and the amount of sulfur source on the formation of CIS, samples with three different concentrations of TU were prepared, each annealed at three different temperatures. Previously it was shown that a certain excess of TU is necessary to compensate the loss of sulfur during pyrolysis,[32] therefore, three different precursor solutions with varying amounts of TU (1.8, 3.1, and 4.5 equiv. TU) were prepared. The Cu/In-ratio was fixed to 1.5 to avoid secondary phases (e.g., In_2S_3)[33−35] and to favor the formation of CIS with chalcopyrite structure and p-type conductivity.[32] The precursor solutions were spin coated (in situ GIWAXS and GISAXS studies, SEM analysis, UV/vis measurements) to obtain thin films and also pneumatically sprayed onto glass substrates (XRD analysis, TEM-EDX analysis, HRMS) to prepare CIS powders. In both cases the precursor layers were annealed at different temperatures (200, 300, and 450 °C) to obtain CIS films.

X-ray Diffraction. For all samples we observed the major X-ray diffraction peaks (112), (220), and (312) characteristic for the chalcopyrite type structure of CIS (Figure 1). Additionally, the XRD patterns obtained at 300 and 450 °C showed the minor superstructure reflections (200), (224), and (440) of the chalcopyrite crystal structure, due to the higher crystallinity of these powders. The positions of the reflections are in good agreement with literature values of crystalline CIS (chalcopyrite), according to the Powder Diffraction File (PDF) 27−159 of the International Centre for Diffraction Data.

The crystallinity of the obtained CIS powders (Table 1) depended strongly on the annealing temperature, as all reflections got sharper with increasing temperature, whereas the concentration of TU has only a minor influence. It had to be noted that the uncertainty of the calculation of the crystallographic domain sizes using Scherrer formula is rather high, thus, it can only be seen as a rough estimation.

No indications for impurities were observed for all CIS powders synthesized at 450 °C. Hence, they can be regarded as single phase with chalcopyrite crystal structure based on the XRD analysis.

Samples prepared with 3.1 equiv. of TU showed no additional reflections, indicating secondary phases, independent from the annealing temperature. However, at low temperatures (200 and 300 °C) the coexistence of traces of amorphous secondary phases or minor impurities cannot be fully ruled out, because of the broadness of the reflections caused by the low crystallinity of these powders.

XRD patterns of samples synthesized with 1.8 equiv. of TU and heat treated at 200 and 300 °C, show an unidentified secondary phase indicated by a not completely symmetrical (220) reflection (compare mark (↓) in Figure 1). We assume

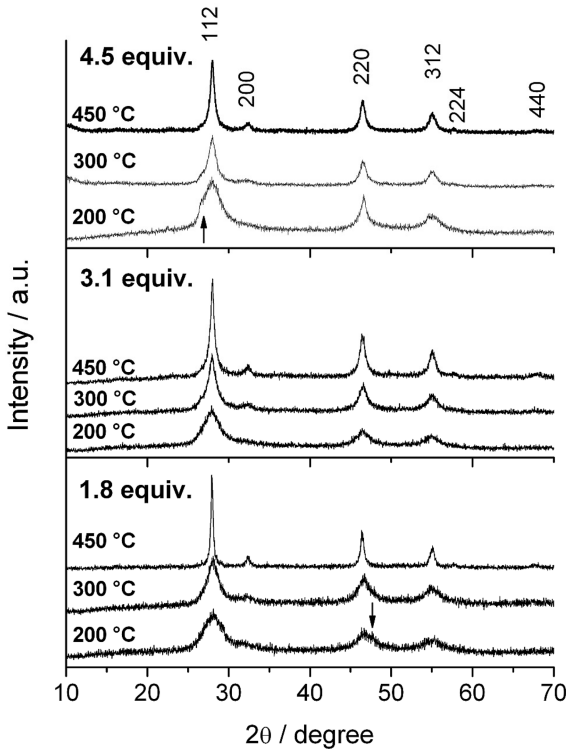

Figure 1. X-ray diffraction patterns of CIS samples prepared with 1.8, 3.1, and 4.5 equiv. of TU at different temperatures. Diffraction patterns are shifted vertically for better visibility. Arrows mark reflections, which do not belong to the chalcopyrite crystal structure.

Table 1. Crystallographic Domain Sizes of CIS Powders Synthesized at Different Temperatures and with Different Equivalents of TU (estimated via Scherrer formula from the XRD-patterns)

	crystallographic domain sizes/nm		
equiv. of TU	200 °C	300 °C	450 °C
1.8	5.0	6.4	23.4
3.1	6.7	8.7	13.8
4.5	5.8	9.9	12.9

that the amount of TU in these samples is not sufficiently high enough to ensure a complete coordination of the copper and indium metal ions, therefore, different kinds of metal complexes might be present. This leads in turn to a nonuniform reaction across the film and to the formation of secondary phases.

Samples prepared at 200 and 300 °C with 4.5 equiv. of TU showed a shoulder at the (112) reflection (compare mark (↑) in Figure 1), which was already mentioned several times in the literature before.[21,33−35] It was observed that these additional reflections were more pronounced when sulfur rich precursor solutions were used, which is consistent with our experiments. It was suggested that they may, at least partially, derive from organic impurities like melamine, melamine acid or cyanuric acid[34] or from indium rich secondary phases (e.g., $CuIn_5S_8$, $CuIn_{11}S_{17}$, In_6S_7 or In_2S_3). In our case, it is very unlikely that this shoulder is caused by indium rich phases as the used Cu/In-ratio should be sufficiently high. The possibility that copper rich phases (CuS, CuS_2 or Cu_7S_4) are responsible is unlikely as the extra reflections occur only for the 4.5 equiv. sample at an annealing temperature of 200 and 300 °C. In contrast to inorganic phases, organic impurities like melamine - formed by the trimerization of TU - seem very plausible.[36] On the one hand, the high concentration of TU in this series (4.5 equiv. of TU) could lead to a pronounced formation of this byproduct and due to its decomposition temperature (>280 °C), the impurity cannot be seen in samples prepared at 450 °C. This assumption is further supported by HRMS measurements, where melamine was detected as byproduct.

In situ GIWAXS and GISAXS Analysis. Results of the XRD analysis discussed above show that samples prepared at 200 °C already possess a chalcopyrite type crystal structure. To obtain information about the temperature at which the reaction − the decomposition of TU and the formation of CIS − starts, we performed a combined time-resolved GIWAXS and GISAXS study on spin-coated precursor films in the temperature range from 40 °C up to 190 °C.

GIWAXS patterns collected during the conversion of a precursor film with 4.5 (left) and 1.8 equiv. of TU (right) are shown in Figure 2.

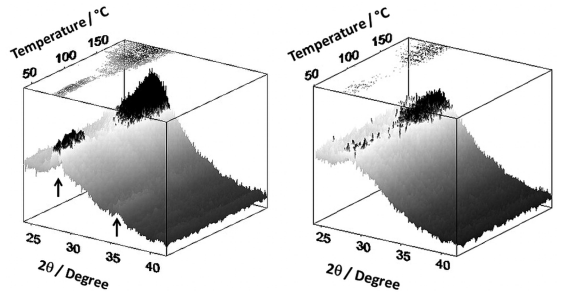

Figure 2. GIWAXS patterns with the corresponding contour plot on top of samples with 4.5 (left) and 1.8 equiv. of TU (right) showing the (112) reflection of the chalcopyrite structure obtained during the heating run with a heating rate of approximately 8 °C min^{-1}.

At room temperature two sharp reflections at approximately 28° and 36° (marked with (↑)) are visible, which may originate from TU- and TU/metal-complexes. This assumption is supported by the fact that these reflections are more intense in the case of the sample with higher TU concentration within the precursor solution. During the heating run these reflections vanish in both cases and a peak at approximately 28° evolves, which can be assigned to the (112) reflection of the CIS chalcopyrite structure, based on results obtained by XRD analysis. In the case of the sample prepared with 4.5 equiv. of TU, the evolving (112) reflection is much sharper, indicating a higher crystallinity than in the case of the sample with the lower concentration of TU.

By plotting the Lorentz corrected integrated intensity ($\int dq q^2 I(q)$) from 26–29° 2θ) versus the temperature (Figure 3), the thermal onset for the evolution of the (112) reflection can be estimated.

The slight variation in intensity between 80 and 130 °C can be assigned to the decomposition of TU or TU/metal complexes, whereas the rapid increase in intensity above 130 °C derives from the appearance of the (112) diffraction peak.

Interestingly, this temperature, 130 °C, is much lower than the decomposition temperature of pure thiourea (approximately 190 °C) or metal salt/thiourea complexes (200 °C),[25,26] indicating a catalytic effect of pyridine for the thermal conversion reaction. This facilitates the decomposition of TU and the generation of sulfur species to form the metal sulfide. Similar observations were made by Fan et al. for the formation of CuS, starting from a precursor solution using pyridine as a solvent.[28]

dx.doi.org/10.1021/am2014579 | ACS Appl. Mater. Interfaces 2012, 4, 382−390

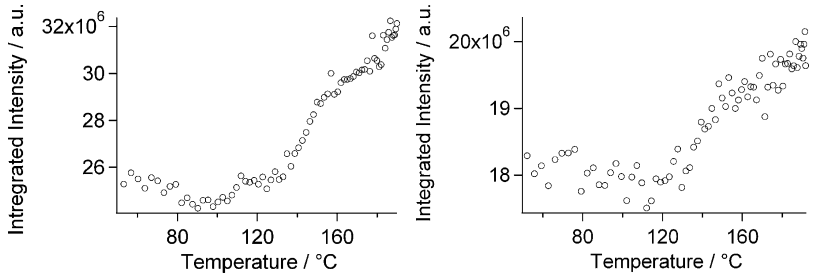

Figure 3. Lorentz corrected integrated intensity (4.5 equiv. of TU, left; 1.8 equiv. of TU, right) calculated from GIWAXS patterns of Figure 2 in the WAXS range between 26 and 29° 2θ, where the (112) reflection of chalcopyrite appears.

To investigate internal changes of the nanostructure of the films during the heating run, in situ GISAXS patterns have been recorded simultaneously with the GIWAXS measurements. Typical results, obtained from a sample with 4.5 equiv. of TU, are shown in Figure 4a and Figure 4b taken at 40 and at 190 °C,

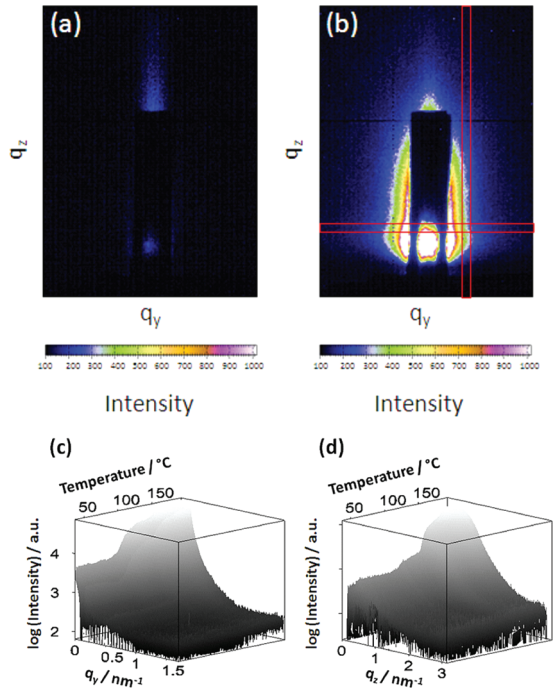

Figure 4. GISAXS patterns of samples prepared with 4.5 equiv. TU (a) at room temperature and (b) at 190 °C. The red squares indicate the vertical and horizontal areas for integration (in-plane and out-of-plane scattering). Evolution of (c) the in-plane scattering and (d) the out-of-plane scattering as a function of temperature.

respectively. Qualitatively the evolution of the GISAXS patterns over the temperature is visualized in Figure 4c, d, in which the in-plane as well as the out-of-plane scattering is presented. Both have been obtained by integration over the boxes as indicated in Figure 4b. In both directions a strong increase of the scattering intensity with temperature is visible attributed to the chemical and/or morphological changes as well as CIS formation and is quantified in detail in the following. Therefore, the out-of-plane data have been analyzed in detail. First, the correlation length[37] has been determined which is defined by

$$l_m = 2\pi \int (qI(q)dq) \Big/ \int (q^2 I(q)dq)$$

and is proportional to a characteristic dimension of the nanoparticles/crystallites. Second, for a profound analysis the data have been fitted with a generalized unified Guinier-exponential/power-law function[38] with polymeric constrain, in which a Porod term accounting for the surface roughness and large inhomogeneities was included. In addition for samples prepared with 4.5 equiv. TU a structure factor had to be included at a later stage, for which a hard-sphere interaction model[39,40] ($S_{Hsp}(q,R_{Hsp},p_{Hsp})$) was used. This was necessary to describe properly the scattering patterns. The whole equation writes as

$$I_{GISAXS}(q_y, q_z) = G\left(\exp\left(-\left(\frac{q^2 R_g^2}{3}\right)\right) + \frac{2}{R_g^2}\left(\frac{\left(\operatorname{erf}\left(\frac{qR_g}{\sqrt{6}}\right)\right)^3}{q}\right)^p\right) \times S_{Hsp}(q, R_{Hsp}, p_{Hsp}) + \frac{C_{por}}{q^{P_{por}}}$$

in which q stands for the scattering vector calculated with $q = (q_y^2 + q_z^2)^{1/2}$. The scattering vectors in-plane and out-of-plane are denoted with q_y and q_z, respectively. G denotes the Guinier prefactor and R_g the radius of gyration. The parameters R_{Hsp} and p_{Hsp} are the hardsphere radius and the volume fraction of the hardsphere, respectively, and determine the structure factor. Both parameters have been fixed in the beginning (R_{Hsp} = 3 nm and p_{Hsp} = 0) and were fitted only when the structurefactor was visible in the scattering pattern. The parameters C_{por} and P_{por}, determine the power-law contribution of the surface roughness and large inhomogeneities. In this simplified approach the influence of refraction and correction terms of the DWBA theory[41] have been neglected, as only the structural progression was the main focus of the study.

The quality of the fits can be observed in Figure 5 (4.5 equiv. of TU) and Figure S1 (1.8 equiv. of TU) − see the Supporting Information − in which the vertical GISAXS cuts are shown together with the fit.

The qualitative behavior can be clearly identified in the correlation length l_m (Figure 6a, d). The small increase of the correlation length below 130 °C indicates chemical or/and morphological changes within the precursor film prior the formation

dx.doi.org/10.1021/am2014579 | ACS Appl. Mater. Interfaces 2012, 4, 382−390

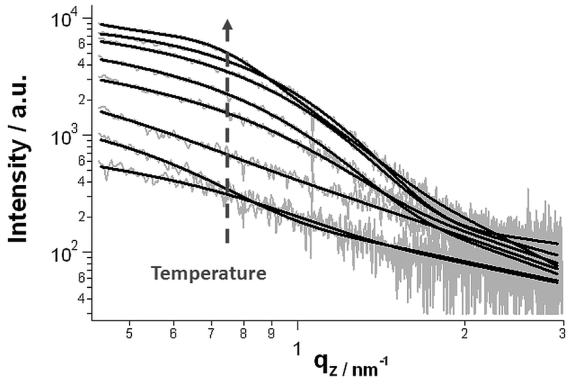

Figure 5. Vertical GISAXS cuts at different temperatures (73, 123, 138, 143, 168, 175, 181, 192 °C) for a sample prepared with 4.5 equiv. of TU and the corresponding fits. The position of interference shoulder caused by the structure factor is indicated with an arrow.

of CIS nanoparticles. At 130 °C a second sharp increase of l_m can be observed, which was attributed to the growth of CIS crystallites. These results underline the findings from the XRD-measurements.

The determined normalized Guinier prefactor G/G_{max} over temperatures (Figure 6c, f) quantifies the qualitative behavior as expected from GIWAXS and in- and out-of-plane GISAXS and manifests the increase of the electron density contrast and particle numbers caused by the CIS formation.

Assuming that the scattering structures are mainly caused by the crystalline phase, and in particular the smallest values of scattering objects are therefore the primary crystallites, the radius of gyration R_g of 3.4 (4.5 equiv. of TU) and 2.6 nm (1.8 equiv. of TU), should be related to the crystal dimensions. Assuming spherical CIS crystallites the diameter can be calculated using the equation $d = 2(5/3)^{1/2}R_g$.[37] The obtained diameter of 8.8 and 6.7 nm, respectively, is in fairly good agreement to the diameter calculated from XRD measurements (6 and 5 nm) taking into account that the Scherrer equation can be seen only as an estimation.

In addition, for samples prepared with 4.5 equiv. of TU, it can be clearly seen that the fit parameters p_{Hsp} and R_{Hsp}, i.e., the structure factor, show a sharp increase at approximately 180 °C, indicating changes in the morphology of the film: the order of the CIS nanoparticles increases suddenly at this temperature.

Summing up the GIWAXS and GISAXS results, we conclude that CIS nanoparticles are already formed at temperatures above 130 °C, however some morphological and/or chemical changes take place already at 90 °C. The morphological changes occurring at 180 °C might be caused by the excess amount of

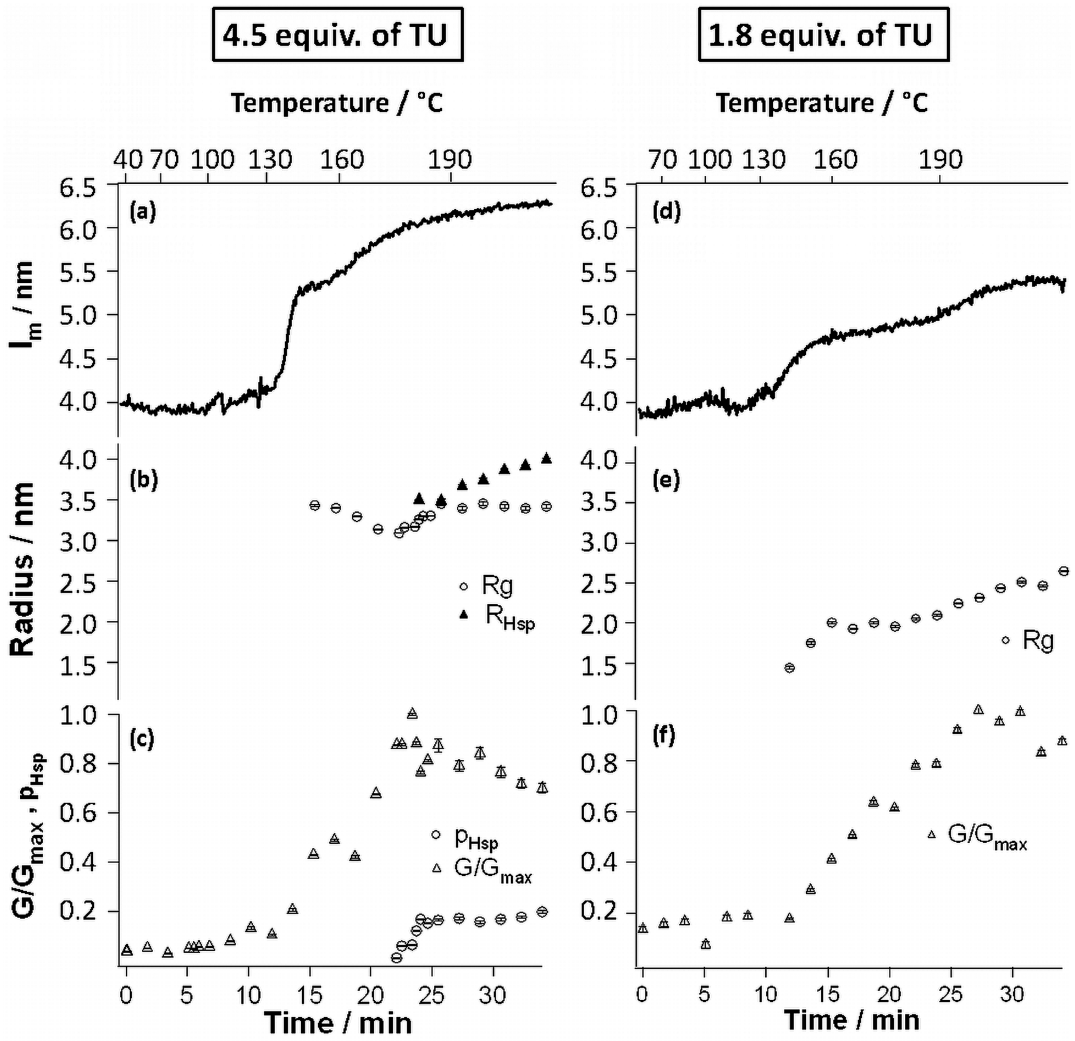

Figure 6. (a–c) Evolution of l_m and fit parameters p_{Hsp}, G, R_g, and R_{Hsp} for a sample prepared with 4.5 equiv. of TU and (d–f) evolution of l_m and fit parameters G and R_g for a sample prepared with 1.8 equiv. of TU during the heating run.

dx.doi.org/10.1021/am2014579 | ACS Appl. Mater. Interfaces 2012, 4, 382–390

TU in the samples with 4.5 equiv. as these observations were not made in samples prepared with 1.8 equiv. TU. To provide evidence for this assumption made on the basis of the GISAXS analysis, we further studied films synthesized at 160 and 220 °C with SEM.

Microstructure Cross-Section. SEM cross sections of CIS thin films annealed at 160 and 220 °C are shown in Figure 7.

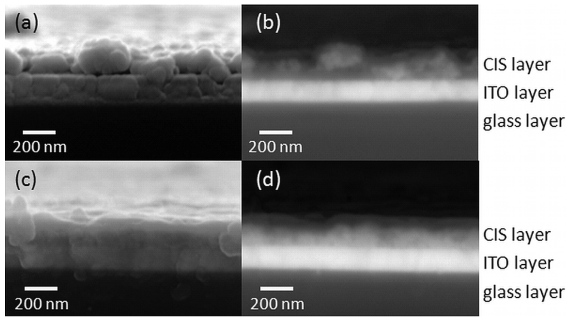

Figure 7. SEM micrographs of a cross-sectional view of a CIS layer synthesized at (a, b) 160 and (c, d) 220 °C with 4.5 equiv. of TU, recorded with a SE-inlens (SE) detector (left) and an angle selective backscattered electron (ASB)-detector (right).

These measurements demonstrate indeed that the morphology of the films changes significantly between these two temperatures.

The nonuniform and cluster-like film at 160 °C turns into a compact film with an even surface at 220 °C. This observation confirms the result obtained by GISAXS measurements.

To reveal these changes at certain stages of the heating process, we performed simultaneous TG/MS analysis.

Simultaneous TG/MS Analysis. Samples were prepared by adding 25 μL of the CIS precursor solution into an Al_2O_3 crucible, which was further stored under vacuum at 60 °C for 8 h. On the one hand, this temperature is low enough to avoid decomposition of precursors, and on the other hand, noncoordinated pyridine can be removed.

Figure 8 gives a comparison of the absolute mass loss of samples prepared with different equiv. of TU and Figure 9

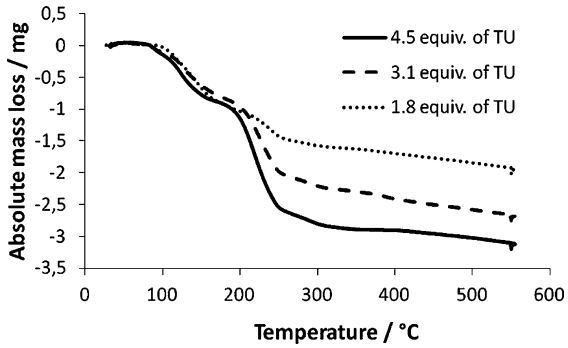

Figure 8. TG curves of samples prepared with 4.5, 3.1, and 1.8 equiv. of TU recorded in flowing helium at a heating rate of 8 °C min^{-1}. The sample mass is 4.5, 3.1, and 2.7 mg, respectively. All samples contain the same quantity of metal salt precursors and only varying amounts of TU.

shows an overlay of the simultaneously recorded TG and TIC traces of a sample prepared with 4.5 equiv. of TU. All samples contain the same amount of metal salt precursors and only varying quantities of TU. The first mass loss starts at approx-

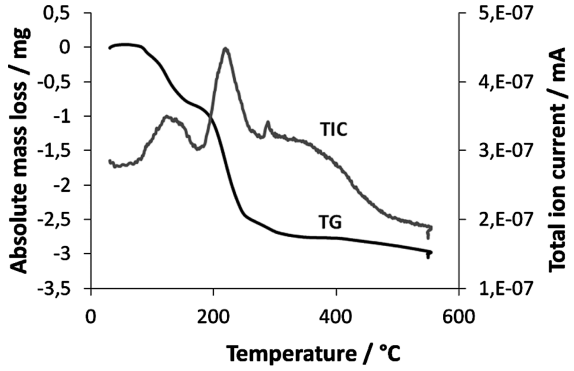

Figure 9. TG curve (black) and total ion current trace (gray) of a sample prepared with 4.5 equiv. of TU as measured in helium with a heating rate of 8 °C min-1 by simultaneous TG/MS. The sample mass is 4.5 mg.

imately 80 °C and was mainly identified as evaporation of pyridine. Pyridine was detected above 80 °C with its maximum evaporation rate at 120 °C, corresponding to its boiling point (bp. 115 °C). It has to be noted that all noncoordinated pyridine was removed during the sample preparation, therefore, it is very likely that the evaporating pyridine derives from decomposing metal salt/TU/pyridine complexes. Based on this result, the onset of the decomposition of the precursors can be expected between 80 and 105 °C. This is in accordance with literature, where CuS was formed at 100 °C using a similar precursor system (CuAc, TU, pyridine)[28] and with the GIWAXS and GISAXS results shown above. Interestingly, no significant amounts of volatile decomposition products of TU were found in this temperature range, despite the fact that evidence for the formation of CIS from 130 °C upward is provided by GIWAXS analysis. From the operational point of view, this temperature is ideal, as it allows obtaining a stable precursor solution and a stable precursor film under ambient conditions. However, the formation of CIS requires only a mild thermal treatment.

The second mass loss between 180 and 260 °C differed remarkably between the samples depending on the used equiv. of TU. In addition, MS data revealed that this weight loss is strongly linked to the evaporation of typical decomposition products of thiourea[27] and thiourea/metal complexes.[26]

On the basis of the combined results from the TG/MS and GIWAXS analysis it can be concluded that sulfur species, necessary for the formation of CIS, are primarily generated by coordinated TU at temperatures below 180 °C. This is reasonable, because at this low temperature range (<130 °C) the decomposition of TU has to be supported catalytically to be able to take place and to allow the generation of sulfur species necessary for the sulfide formation. This catalytical effect can be achieved by the formation of such complexes in combination with the coordinating solvent pyridine. Above 180 °C, the temperature is sufficiently high for the decomposition of noncoordinated thiourea, which is consistent with values from the literature.[27] Supported by these results the morphological changes observed in cross-sectional SEM micrographs of thin films and during GISAXS measurements can be clearly linked to the decomposition of noncoordinated TU. Additionally, this explains why samples with only 1.8 equiv. of TU do not show such a pronounced change in morphology at 180 °C during GISAXS analysis, as these samples possess hardly any noncoordinated TU.

Chemical Composition. The elemental composition was determined using TEM-EDX analysis. Figure 10 shows the

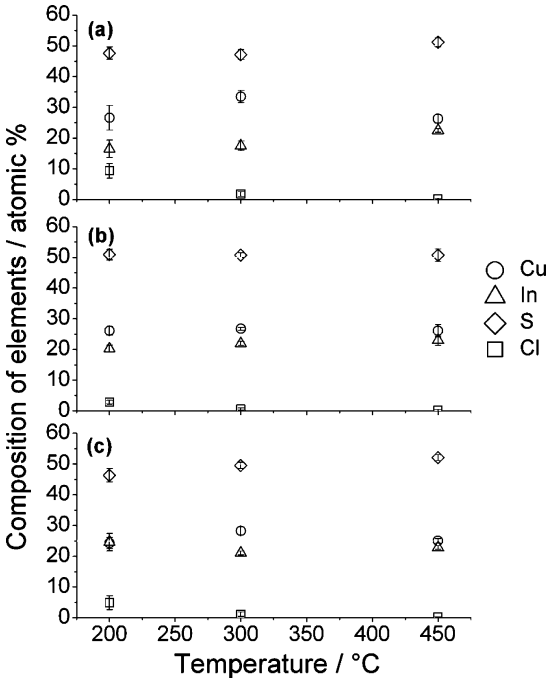

Figure 10. Chemical composition of CIS powders prepared with (a) 1.8, (b) 3.1, and (c) 4.5 equiv. of TU in the precursor solution. The horizontal gray lines correspond to the theoretical value of S (dashed line) and Cu and In (dotted line) for stoichiometric CIS.

atomic percentage of the elements for the prepared CIS samples. The atom percentages were calculated using the Cu K, Zn K, Sn L, and S K peaks using the Cliff–Lorimer approximation.[42] The elemental ratios of Cu/In and S/(Cu+In) are summarized in Table 2. All CIS powders possess nearly stoichiometric amounts of sulfur, with a S/(Cu+In) ratio varying between 0.93 and 1.11, independent from the concentration of TU in the precursor solution or the annealing temperature. In contrast to CIS powders prepared with 3.1 and 4.5 equiv. of TU, the stoichiometry of samples prepared with 1.8 equiv. of TU varies significantly, especially at low annealing temperatures (200 and 300 °C). We assume that this nonuniform elemental distribution across the film is caused by an incomplete coordination of the copper and indium ions by TU (see discussion of XRD analysis).

Except these two cases, all other samples show a lower Cu/In ratio than in the precursor solution (Cu/In = 1.46). These deviations from the starting composition might be caused by a preferred generation of volatile Cu-species during the thermal induced CIS formation when Cu-rich precursor solutions are used.[33] Despite this effect, the samples are still of Cu-rich nature in our case, yielding CIS with p-type conductivity.[1]

Samples prepared at 200 °C exhibit chlorine as an impurity, which may derive from not yet removed decomposition products of the precursor at this stage. However, at higher annealing temperatures (>300 °C) the chlorine content is significantly reduced and samples prepared at 450 °C can be regarded as chlorine-free.

Optical Properties. The optical properties of the synthesized CIS films were studied by transmittance and reflectance measurements. The absorption coefficient (α) was calculated according to following equation[43,44]

$$\alpha = \frac{1}{d}\ln\left(\frac{1-R}{T}\right)$$

where d is the thickness of the film, R the reflectance, and T the transmittance of the film. Figure 11 gives the typical absorption

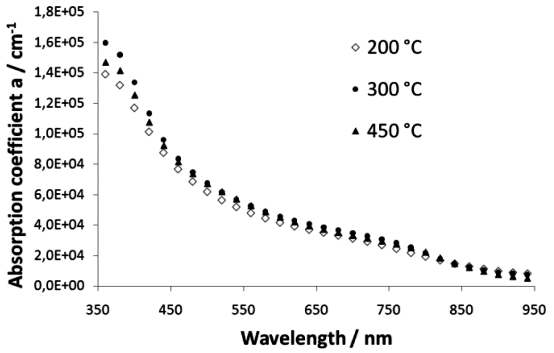

Figure 11. Optical absorption coefficient of CIS films synthesized with 3.1 equiv. of TU and annealed at different temperatures.

spectra obtained for CIS samples annealed at different temperatures using 3.1 equiv. of TU within the precursor solution. In general, it can be seen that all films show a high optical absorption (>1 × 10^4 cm^{-1}) between 350 and 850 nm and very similar absorption spectra independent of the synthesis parameters.

The optical band gap (E_g) values were obtained from the equation:

$$\alpha = \frac{A(h\nu - E_g)^n}{h\nu}$$

where A is a constant, $h\nu$ the photon energy and n an exponent, which is equal to 2 or 1/2 for indirect or direct transition, respectively. In the present work, n was found to be 1/2 indicating a direct band gap, which is consistent with the literature.[21] Therefore, the band gap values were estimated from the $(\alpha h\nu)^2$ versus $(h\nu)$ plots by extrapolating the linear part of the function as shown in Figure 12.

Table 3 gives a summary of the estimated optical band gaps of the prepared CIS films.

The obtained band gaps range from 1.45 to 1.51 eV and do not show a strong dependence on the annealing temperature or

Table 2. Elemental Ratios of the CZTS Powders Synthesized at Different Temperatures Calculated from TEM-EDX Measurements

	elemental ratio					
	1.8 equiv. TU		3.1 equiv. TU		4.5 equiv. TU	
T (°C)	Cu/In	S/(Cu+In)	Cu/In	S/(Cu+In)	Cu/In	S/(Cu+In)
200	1.69 ± 0.51	1.11 ± 0.07	1.29 ± 0.11	1.10 ± 0.08	1.00 ± 0.18	0.95 ± 0.07
300	1.93 ± 0.26	0.93 ± 0.06	1.22 ± 0.04	1.04 ± 0.03	1.34 ± 0.09	1.01 ± 0.04
450	1.17 ± 0.08	1.05 ± 0.06	1.14 ± 0.15	1.03 ± 0.08	1.09 ± 0.04	1.09 ± 0.04

dx.doi.org/10.1021/am2014579 | ACS Appl. Mater. Interfaces 2012, 4, 382–390

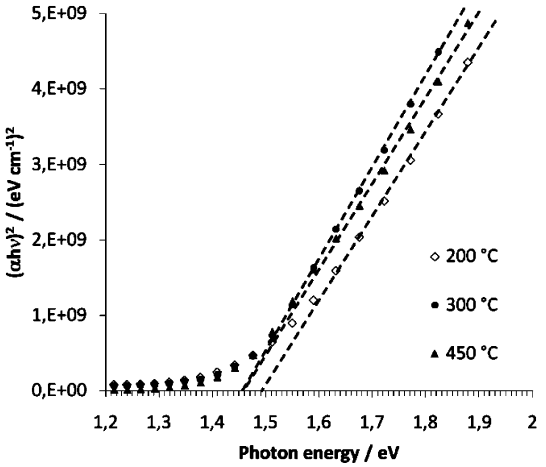

Figure 12. $(\alpha h\nu)^2$ vs photon energy $(h\nu)$ of CIS films prepared with 3.1 equiv. of TU and annealed at different temperatures.

Table 3. Estimated Optical Band Gaps from $(\alpha h\nu)^2$ vs. Photon Energy $(h\nu)$ Plots of Prepared CIS Films

	band gap (eV)		
equiv. of TU	200 °C	300 °C	450 °C
1.8	1.51	1.46	1.48
3.1	1.47	1.47	1.45
4.5	1.49	1.46	1.46

the amount of TU used in the precursor solution. The band gap values are consistent with the literature.[15,21,45]

CONCLUSION

In this paper, we present the preparation of $CuInS_2$ thin films by a chemical deposition method using copper(I) acetate and indium(III) chloride as metal salt precursors, thiourea as sulfur source, and pyridine as solvent. The obtained films are promising for photovoltaic applications as they possess a chalcopyrite crystal structure, a near ideal band gap, and a high absorption coefficient. Additionally, the formation process taking place during the thermal conversion of the precursor layer was studied intensively. The proposed events, which take place during the formation of the CIS layer, are summarized in Figure 13. At the

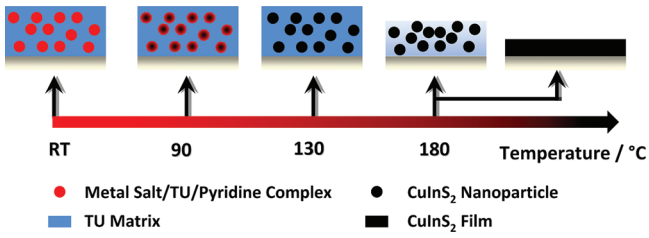

Figure 13. Events occurring during the annealing process and the formation of the $CuInS_2$ thin films.

beginning, the precursor layer consists of metal salt/thiourea/pyridine complexes embedded into a matrix of thiourea. The dimensions of this matrix depend on the equivalents of thiourea used for the preparation of the precursor solution. At 90 °C these metal salt/thiourea/pyridine complexes start to decompose followed by the formation of $CuInS_2$ nanoparticles within the thiourea matrix at 130 °C. This temperature range is much lower than the decomposition temperature of metal salt/thiourea complexes (200 °C) or noncoordinated thiourea (>190 °C), indicating a catalytic effect of pyridine. The thiourea matrix decomposes at 180 °C, which causes the formation of a dense $CuInS_2$ thin film. Hence, it can be concluded that the formation of $CuInS_2$ is primarily linked to the decomposition of thiourea originating from metal salt/thiourea/pyridine complexes. In addition, mass spectrometry studies of CIS powders revealed that melamine is formed as a byproduct.

ASSOCIATED CONTENT

Supporting Information

Additional GISAXS data. This material is available free of charge via the Internet at http://pubs.acs.org/.

AUTHOR INFORMATION

Corresponding Author

*E-mail: thomas.rath@tugraz.at (T.R.); gregor.trimmel@tugraz.at (G.T.). Tel +43-316-87332281. Fax +43-316-873-32302.

ACKNOWLEDGMENTS

The authors thank the Christian Doppler Research Association (CDG), the federal ministry of Economy, Family and Youth of Austria and Isovoltaic AG for financial support. GIWAXS/GISAXS experiments leading to these results have received funding from the European Community's Seventh Framework Programme (FP7/2007-2013) under Grant 226716. In addition, the authors thank J. Schlegl and G. Daemon for their help constructing the GIWAXS/GISAXS temperature controlled heating cell.

REFERENCES

(1) Lewerenz, H. J. *Sol. Energy Mater. Sol. Cells* **2004**, *83*, 395−407.
(2) Merdes, S.; Mainz, R.; Klaer, J.; Meeder, A.; Rodriguez-Alvarez, H.; Schock, H. W.; Lux-Steiner, M. C.; Klenk, R. *Sol. Energy Mater. Sol. Cells* **2011**, *95*, 864−869.
(3) Meyer, N.; Meeder, A.; Schmid, D. *Thin Solid Films* **2007**, *515*, 5979−5984.
(4) Yoshino, K.; Ikari, T.; Shirakata, S.; Miyake, H.; Hiramatsu, K. *Appl. Phys. Lett.* **2001**, *78*, 742−744.
(5) Siebentritt, S. *Thin Solid Films* **2002**, *403*−*404*, 1−8.
(6) Kazmerski, L. L.; Ayyagari, M. S.; Sanborn, G. A. *J. Appl. Phys.* **1975**, *46*, 4865−4869.
(7) Zribi, M.; Kanzari, M. *Thin Solid Films* **2011**, *519*, 3865−3869.
(8) Ogawa, Y.; Uenishi, S.; Tohyama, K.; Ito, K. *Sol. Energy Mater. Sol. Cells* **1994**, *35*, 157−163.
(9) Hwang, H. L.; Cheng, C. L.; Liu, L.; M. Liu, Y. C.; Sun, C. Y. *Thin Solid Films* **1980**, *67*, 83−94.
(10) He, Y, B.; Krost, A.; Blasing, J.; Kriegseis, W.; Polity, A.; Meyer, B., K.; Kisielowski, C. *Thin Solid Films* **2004**, *451*−*452*, 229−232.
(11) Hwang, H.; Tseng, B.; Sun, C.; Loferski, J. *Sol. Energy Mater.* **1980**, *4*, 67−79.
(12) Lee, S. S.; Seo, K. W.; Park, J. P.; Kim, S. K.; Shim, I.-W. *Inorg. Chem.* **2007**, *46*, 1013−7.
(13) Kärber, E.; Katerski, A.; Oja Acik, I.; Mikli, V.; Mere, A.; Krunks, M. *Thin Solid Films* **2011**, *519*, 7180−7183.
(14) Terasako, T.; Uno, Y.; Inoue, S.; Kariya, T.; Shirakata, S. *Phys. Status Solidi C* **2006**, *3*, 2588−2591.
(15) Sharma, A. K.; Rajaram, P. *Mater. Sci. Eng.* **2010**, *172*, 37−42.
(16) Aksay, S.; Altıokka, B. *Phys. Status Solidi C* **2007**, *4*, 585−588.
(17) Mahendran, C.; Suriyanarayanan, N. *Phys. B* **2010**, *405*, 2009−2013.
(18) John, T, T.; Meril, M.; Kartha, S, C.; Vijayakumar, K.; Abe, T.; Kashiwaba, Y. *Sol. Energy Mater. Sol. Cells* **2005**, *89*, 27−36.
(19) Sebastian, T.; Jayakrishnan, R.; Kartha, C. S.; Vijayakumar, K. P. *Open Surf. Sci. J.* **2009**, *1*, 1−6.

(20) Krunks, M.; Kijatkina, O.; Mere, A.; Varema, T.; Oja, I.; Mikli, V. *Sol. Energy Mater. Sol. Cells* **2005**, *87*, 207−214.
(21) Krunks, M.; Bijakina, O.; Varema, T.; Mikli, V.; Mellikov, E. *Thin Solid Films* **1999**, *338*, 125−130.
(22) Li, L.; Coates, N.; Moses, D. *J. Am. Chem. Soc.* **2010**, *132*, 22−23.
(23) Krebs, F. C.; Tromholt, T.; Jorgensen, M. *Nanoscale* **2010**, *2*, 873−886.
(24) Rath, T.; Edler, M.; Haas, W.; Fischereder, A.; Moscher, S.; Schenk, A.; Trattnig, R.; Sezen, M.; Mauthner, G.; Pein, A.; Meischler, D.; Bartl, K.; Saf, R.; Bansal, N.; Haque, S. A.; Hofer, F.; List, E. J. W.; Trimmel, G. *Adv. Energy Mater.* **2011**, *1*, 1046−1050.
(25) Krunks, M.; Leskela, T.; Niinisto, L. *Jpn. J. Appl. Phys.* **2000**, *39*, 181−186.
(26) Madarász, J.; Krunks, M.; Niinisto, L.; Pokol, G. *J. Therm. Anal. Calorim.* **2004**, *78*, 679−686.
(27) Wang, S.; Gao, Q.; Wang, J. *J. Phys. Chem. B* **2005**, *109*, 17281−17289.
(28) Fan, L.; Song, H.; Liu, L.; Zhao, H.; Pan, G.; Jiang, J.; Dong, B.; Bai, X. *J. Nanosci. Nanotechnol.* **2009**, *9*, 2014−2022.
(29) Pradhan, N.; Katz, B.; Efrima, S. *J. Phys. Chem. B* **2003**, *107*, 13843−13854.
(30) Amenitsch, H.; Rappolt, M.; Kriechbaum, M.; Mio, H.; Laggner, P.; Bernstorff, S. *J. Synchrotron Radiat.* **1998**, *5*, 506−508.
(31) Fischereder, A.; Rath, T.; Haas, W.; Amenitsch, H.; Albering, J.; Meischler, D.; Larissegger, S.; Edler, M.; Saf, R.; Hofer, F.; Trimmel, G. *Chem. Mater.* **2010**, 3399−3406.
(32) Tiwari, A.; Pandya, D, K.; Chopra, K, L. *Thin Solid Films* **1985**, *130*, 217−230.
(33) Krunks, M.; Mikli, V.; Bijakina, O.; Mellikov, E. *Appl. Surf. Sci.* **1999**, *142*, 356−361.
(34) Krunks, M.; Mikli, V.; Bijakina, O.; Rebane, H.; Mere, A.; Varema, T.; Mellikov, E. *Thin Solid Films* **2000**, *361−362*, 61−64.
(35) Ortega-López, M.; Morales-Acevedo, A. *Thin Solid Films* **1998**, *330*, 96−101.
(36) Maier, E.; Rath, T.; Haas, W.; Werzer, O.; Saf, R.; Hofer, F.; Meissner, D.; Volobujeva, O.; Bereznev, S.; Mellikov, E.; Amenitsch, H.; Resel, R.; Trimmel, G. *Sol. Energy Mater. Sol. Cells* **2011**, *95*, 1354−1361.
(37) Svergun, D. I.; Feigin, L. A. *Structure Analysis by Small-Angle X-ray and Neutron Scattering*; Taylor, G. W., Ed.; Plenum Press: New York, 1987.
(38) Beaucage, G. *J. Appl. Crystallogr.* **1995**, *28*, 717−728.
(39) Pedersen, J. S. *Adv. Colloid Interface Sci.* **1997**, *70*, 171−210.
(40) Kinning, D. J.; Thomas, E. L. *Macromolecules* **1984**, *17*, 1712−1718.
(41) Tolan, M. *X-ray Scattering from Soft-Matter Thin Films*; Springer: Berlin, 1999; Vol. *148*.
(42) Cliff, G.; Lorimer, G, W. *J. Microsc.* **1975**, *103*, 203−207.
(43) Wakkad, M. M.; Shokr, E. K.; Abd El Ghani, H. A.; Awad, M. A. *Eur. Phys. J.* **2008**, *43*, 23−30.
(44) Khemiri, N.; Akkari, F., C.; Kanzari, M.; Rezig, B. *Phys. Status Solidi A* **2008**, *205*, 1952−1956.
(45) Guezmir, N.; Ouerfelli, J.; Belgacem, S. *Mater. Chem. Phys.* **2006**, *96*, 116−123.